Journal of Biomedical Informatics 132 (2022) 104121

Contents lists available at ScienceDirect

Journal of Biomedical Informatics

journal homepage: www.elsevier.com/locate/yjbin

Realistic 3D infant head surfaces augmentation to improve AI-based diagnosis of cranial deformities

Helena R. Torres [a,b,c,d,*], Bruno Oliveira [a,b,c,d], Pedro Morais [a], Anne Fritze [e], Mario Rüdiger [e], Jaime C. Fonseca [b], João L. Vilaça [a]

[a] 2Ai – School of Technology, IPCA, Barcelos, Portugal
[b] Algoritmi Center, School of Engineering, University of Minho, Guimarães, Portugal
[c] Life and Health Sciences Research Institute (ICVS), School of Medicine, University of Minho, Braga, Portugal
[d] ICVS/3B's - PT Government Associate Laboratory, Braga/Guimarães, Portugal
[e] Department for Neonatology and Pediatric Intensive Care, University Hospital Carl Gustav Carus, TU Dresden, Germany

ARTICLE INFO

Keywords:
3D data augmentation
Morphable models
Deep learning
Head deformities
Motion transformation

ABSTRACT

Evaluation of the head shape of newborns is needed to detect cranial deformities, disturbances in head growth, and consequently, to predict short- and long-term neurodevelopment. Currently, there is a lack of automatic tools to provide a detailed evaluation of the head shape. Artificial intelligence (AI) methods, namely deep learning (DL), can be explored to develop fast and automatic approaches for shape evaluation. However, due to the clinical variability of patients' head anatomy, generalization of AI networks to the clinical needs is paramount and extremely challenging. In this work, a new framework is proposed to augment the 3D data used for training DL networks for shape evaluation. The proposed augmentation strategy deforms head surfaces towards different deformities. For that, a point-based 3D morphable model (p3DMM) is developed to generate a statistical model representative of head shapes of different cranial deformities. Afterward, a constrained transformation approach (3DHT) is applied to warp a head surface towards a target deformity by estimating a dense motion field from a sparse one resulted from the p3DMM. Qualitative evaluation showed that the proposed method generates realistic head shapes indistinguishable from the real ones. Moreover, quantitative experiments demonstrated that DL networks training with the proposed augmented surfaces improves their performance in terms of head shape analysis. Overall, the introduced augmentation allows to effectively transform a given head surface towards different deformity shapes, potentiating the development of DL approaches for head shape analysis.

1. Introduction

Evaluation of head shape is a topic of significant interest in pediatrics since head deformities can indicate or cause disturbed neuro-cognitive development [1–3]. Conditions associated with poor neuro-development are disturbances of head growth, which can indicate defects in the brain size and skull malformations, and the presence of cranial deformities. Cranial deformities are characterized by an abnormal infant's head shape, which can refer to an asymmetric flattening of the skull (*i.e.* asymmetrical deformations) or a parietal widening/elongation of the head (*i.e.* symmetric deformation) [4–6] (Fig. 1). The incidence of head distortions among term-born infants is indicated to be 20%, increasing up to 38% in preterm infants [7,8]. Thus, evaluation of head shape and appropriate monitoring is paramount for improving long-term outcomes. Currently, head shape evaluation is performed through visual inspection or using cranial anthropometric measurements, which can be manually obtained using calipers or obtained from 3D head surfaces generated by 3D digital techniques or medical imaging [9–11]. However, the head shape evaluation process is time-consuming and highly dependent on the observer's expertise, being sub-optimal and susceptible to errors [12]. Moreover, even when using 3D digital surfaces for shape analysis, only 2D anthropometric measurements are estimated using landmarks manually placed by one observer, failing to correctly characterize the 3D head shape. Thus, automatic tools for performing a detailed head shape evaluation are claimed.

Artificial intelligence (AI) techniques, namely deep learning (DL), already demonstrated their crucial role in aiding clinicians to perform

* Corresponding author.
E-mail address: htorres@ipca.pt (H.R. Torres).

https://doi.org/10.1016/j.jbi.2022.104121
Received 20 December 2021; Received in revised form 31 May 2022; Accepted 11 June 2022
Available online 22 June 2022

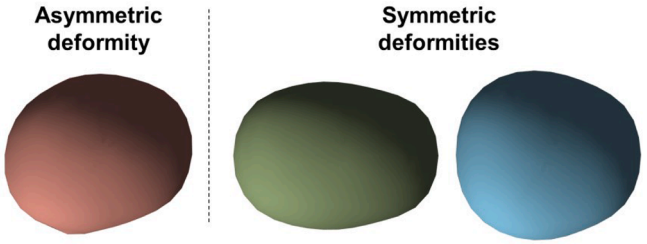

Fig. 1. Top view of different types of cranial deformities. Red head: Plagiocephaly; Green head: Scaphocephaly; Blue head: Brachycephaly.

several medical tasks, such as diagnosis, monitoring, treatment planning, or treatment outcome prediction [13–15]. To accurately train these DL approaches, large amounts of data are needed which is challenging in the medical field. Concerning the task of human head modeling, a number of publicly available datasets have been released. Most of them are only related to facial surfaces, e.g. the Large Scale Facial Model (LSFM) [16], the FRGC dataset [17], the Bosphorus 3D face dataset [18], or the Basel Face Model [19], precluding their usage for head shape analysis. Few datasets of the complete human head were also released, namely the Liverpool-York Head Model (LYHM) [20], the FLAME dataset [21], or the Large scale Face-and-Head Model, which combines the LYHM with the LSFM [22]. However, these datasets are mostly focused on the adult population, failing to capture the particularities of newborns and/or infants. More importantly, these datasets are mainly focused on normal head shapes and do not contain head shapes with cranial deformities. Thus, the application of these datasets for the development of automatic methods for infant cranial deformity detection is limited. In fact, the availability of medical data with specific disorders, *e.g.* cranial deformities, is difficult. Moreover, even when data is available, the process of manual labeling is also a tedious and complex task, especially for 3D data [23]. To solve this problem, data augmentation strategies are frequently applied, increasing the size and variability of a given dataset by introducing variations to the original data. This allows to reduce the overfitting and improves the generalization ability of the network, increasing its accuracy [24]. Concerning 3D surfaces, traditional augmentation techniques often rely on simple geometric transformations (such as flipping, rotations, or scalings) or small perturbations on the surface points [25]. Recently, an adversarial learning strategy denominated PointAugment was proposed by Li et al. to augment point clouds [26]. Here, an adversarial learning strategy is applied to jointly train an *augmentor* and a classifier network, such that the *augmentor* can learn how to generate augmented data. In [27], an augmentation based on locally weighted deformations was proposed. In the work of Chen et al., point-cloud augmentation was also studied, where the augmentation is performed by interpolating two objects [28]. However, for the task of head shape analysis, where different head deformities with multiple severities are clinically relevant, the traditional augmentation techniques (mostly based on geometric transformations) may not be enough to generate realistic data targeting this specific application. Moreover, although the state-of-the-art augmentation techniques can be parametrized, it is difficult to control the final augmentation forms towards target deformities, potentially leading to undesired or unexpected shapes. Another approach that can be used for augmentation is the 3D morphable models (3DMM) [29,30]. 3DMM are statistical models that capture the variations of shapes of a given population through Principal Component Analysis (PCA) [31]. By varying its parameters, the model can be morphed and new shapes can be generated. However, the variability of the shapes generated is directly correlated with the number of shapes used to construct the statistical model, limiting the augmentation to the anatomical variability available in the population. Thus, instead of using 3DMM as a direct augmentation approach, state-of-the-art methods focused on fitting techniques (*i.e.,* fitting the statistical models to new data using for example anthropometric landmarks) were used to deform the original model and augment it [29].

This work focuses on the development of a novel data augmentation strategy to generate head surfaces with different cranial deformities. For that, a constrained transformation approach (3DHT) is applied to transform a head surface to a desired deformity. The target deformity is represented by a point-based 3D morphable model (p3DMM) constructed to represent cranial shape variations of a population with a given deformity. The p3DMM is the basis for the calculation of a motion field that guides the transformation.

The contributions of this work can be described as follows:

- Development of a novel methodology to transform a head surface to a target deformity, allowing to augment the surfaces to different shapes and deformities. To the best of our knowledge, the creation of head surfaces with different deformities has not yet been described in the literature. The proposed framework software is available on our website[1].
- Creation of a new point-based 3DMM, the p3DMM, that uses anatomically defined control points to represent shape variability. This strategy avoids the need for highly detailed shape surfaces while maintaining the shape significance of the statistical model. Moreover, the use of control points provides flexibility and speeds up the transformation process.
- Development of a transformation methodology to promote the warping between a head surface and a point-based statistical model using dense motion transformations;
- Validation of the potential of the proposed data augmentation approach in DL applications that can be used for head shape analysis, namely automatic classification of a head shape concerning cranial deformities, part head segmentation, and anthropometric landmark detection.

The remainder of the paper is structured as follows. In section 2, the proposed augmentation methodology is described. The experiments performed are described in section 3, with the results presented in section 4. In section 5, the augmentation method is discussed, and the conclusions are presented in section 6.

2. Methods

2.1. Overview

In this section, the proposed 3D data augmentation method is described (Fig. 2). The initial stage of the method consists of constructing a p3DMM to statistically represent a population with a given cranial deformity. The p3DMM is used to create a sparse motion field between the target deformity, implicitly incorporated in the p3DMM, and the head surface to be deformed. From the sparse motion field, a complete and smooth dense motion field is estimated using gaussian modeling. A constrained transformation approach is iteratively applied using the dense motion field to perform the surface warping.

2.2. Point-based 3D morphable model (p3DMM)

The proposed data augmentation approach relies on a target shape towards which a head surface will be deformed. To produce different target shapes and deformities, a 3DMM-based approach is proposed, where a statistical model for each cranial deformity is constructed from a set of sample head surfaces. Particularly in this study, five different types of head shapes were used, namely plagiocephaly (Pl), brachycephaly (Bl), scaphocephaly (Sc), combined plagiocephaly and brachycephaly (PlBr), and no deformity (normal head shape, Nl) (see Fig. 1).

[1] https://myneurogrowth.ipca.pt/index.php/the-expected-outputs/.

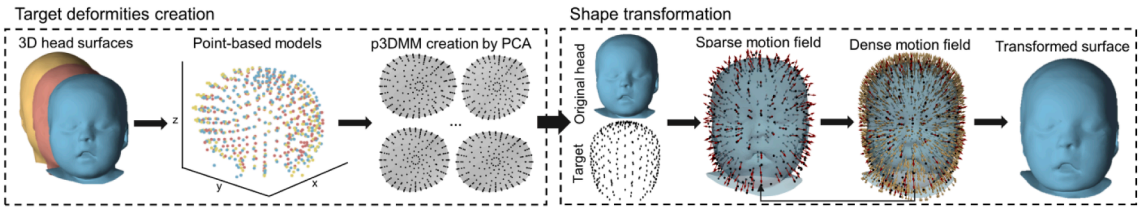

Fig. 2. Overview of the proposed augmentation approach.

2.2.1. Head surface correspondence

In traditional 3DMM, the construction of the statistical shape model relies on a dense point-to-point correspondence of the surfaces, where each point has the same semantic representation across all surfaces [30]. This means that each identity on the surface (e.g., inner and outer corners of the eyes, tip of the nose, or mouth corners) are represented in a particular vertex in all the meshes, allowing the use of PCA to analyze variations of the population. In this work, the overall shape of the surfaces is studied, instead of particular features of the face/head. Thus, a coarse point-to-point correspondence is applied.

To perform the coarse point-to-point correspondence, a point-based head model representative of the head, *i.e.,* that maintains its shape significance, is constructed for each surface (Fig. 3). Firstly, each head surface is affinely aligned to a reference one using an Iterative Closest Point (ICP) method guided by anthropometric landmarks labeled in each head. To compensate for head size differences, all head surfaces were initially normalized to be contained in a unit sphere without changing its height/length/width relation. Once performed the coarse matching, the origin (o) of each head surface is defined as the mean point between two landmarks placed at each ear (*i.e.*, the tragions). From o, a ray casting algorithm is applied to find points on the head surface at specific orientations. Specifically, rays are emitted from the surface's origin o in angles that vary between 0 and 360 degrees in the azimuthal plane and -90 to 90 degrees in the zenithal plane, covering the entire region around the head. Afterward, the Ray-Triangle Intersection method proposed in [32] is applied to construct the *point-based head model* consisting of the intersection points. Thus, each model is defined by a vector $M = [p_1, p_2, \cdots, p_N] \in \mathbb{R}^{3N}$, where N is the number of rays and $p_i = [p_{ix}, p_{iy}, p_{iz}]$ describes the coordinates of the i-th ray intersection point.

The point-based head models are used to construct the statistical model representative of each head deformity. Since the head surfaces are rigidly aligned to a common space and rays with the same directions are used across all surfaces, each point of the point-based models coarsely represents the same anatomical region. Thus, PCA can be applied for statistical model construction.

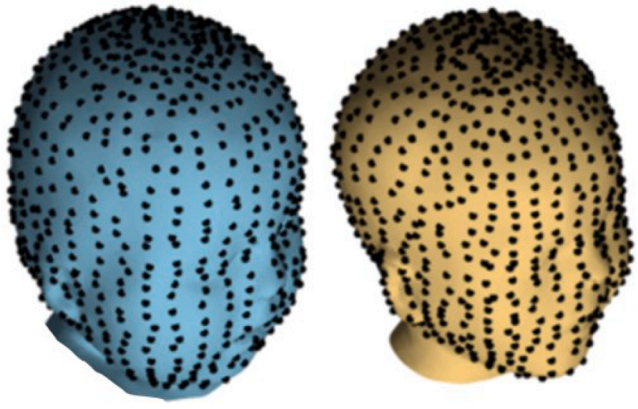

Fig. 3. Head surfaces with the respective point-based models represented by the black dots.

2.2.2. Point-based statistical modeling

The point-based models are statistically analyzed by PCA to generate deformity-specific point-based morphable models expressed as a linear basis of the shapes [33]. Let us represent each point-based model as the representation vector M. From the representation vectors, a matrix V with shape $S \times 3N$ is then defined as $V = [{M_1}^T, \cdots, {M_S}^T]^T$, where S represents the number of samples of head surfaces. From this, different shape instances V' can be generated using:

$$V' = \overline{V} + Eb, \tag{1}$$

where $\overline{V} \in \mathbb{R}^{3N}$ is the mean shape model and $E \in \mathbb{R}^{3N \times (S-1)}$ is the orthonormal basis matrix that contains the shape eigenvectors of the covariance matrix of V, ordered with respect to the corresponding eigenvalues. Also, $b \in \mathbb{R}^{S-1}$ is a vector of shape parameters that define a shape instance under the morphable model [16]. In Fig. 4, the surfaces enclosed by the principal components of the p3DMMs are presented. Since different head shapes and severities are represented in each p3DMM, different target deformities can be retrieved from the models. Furthermore, although specific details are not represented in the p3DMM (e.g., facial features), the overall shape needed for the augmentation process is maintained.

2.3. 3D head transformation approach (3DHT)

At this stage, a transformation method that uses a motion displacement field strategy to warp a given head surface towards a target deformity is applied. For that, a sparse motion field is computed at control points of the surface. These control points are defined from the point-based model of the head. Afterward, a constrained dense displacement field is estimated for all surface points (Fig. 5).

2.3.1. Motion displacement field estimation

As abovementioned, control points are used as reference points for the transformation process. Concerning the head to be deformed, the control points to be moved are defined to be its point-based head model, M_m, estimated as described previously. The target control points are defined to be a given variation mode of the p3DMMs, M_t. Here, M_t is a shape instance estimated using equation (1). During the transformation process, the moving points are warped towards the target ones. Since both moving and target points are in coarse correspondence, a motion displacement field $\{u_s, v_s, k_s\}$ that allows to move M_m towards M_t can be computed. This sparse displacement field, *i.e.* computed only over the domain of the point-based model, can be given by:

$$\{u_s(p_i), v_s(p_i), k_s(p_i)\} = \{x_{mi} - x_{ti}, y_{mi} - y_{ti}, z_{mi} - z_{ti}\}, \tag{2}$$

where (x_{mi}, y_{mi}, z_{mi}) and (x_{ti}, y_{ti}, z_{ti}) correspond to the 3D coordinates of the point p_i of M_m and M_t, respectively.

Following the computation of the sparse motion displacement field, a dense motion field defined over the entire moving head is retrieved. For that, a strategy based on Gaussian modeling is applied to populate the dense map for each remaining surface's point j. Let us define a distribution function as $g_i(x; \mu_i, \sigma_i)$ which represents a Gaussian function centered at μ_i and with a variance σ_i. If a function g_i is computed for each

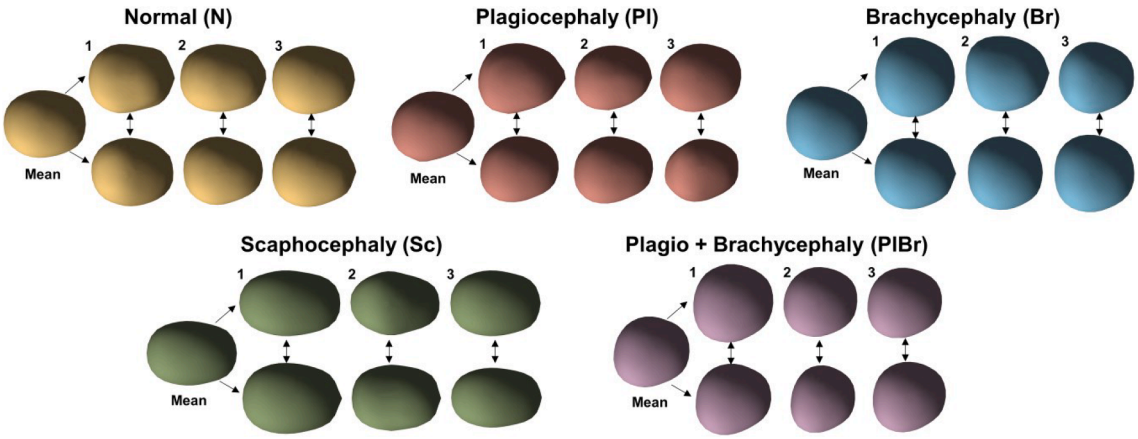

Fig. 4. Surfaces enclosed by each p3DMM. Each p3DMM represents a cranial deformity. The first three shape components along with the mean shapes are presented.

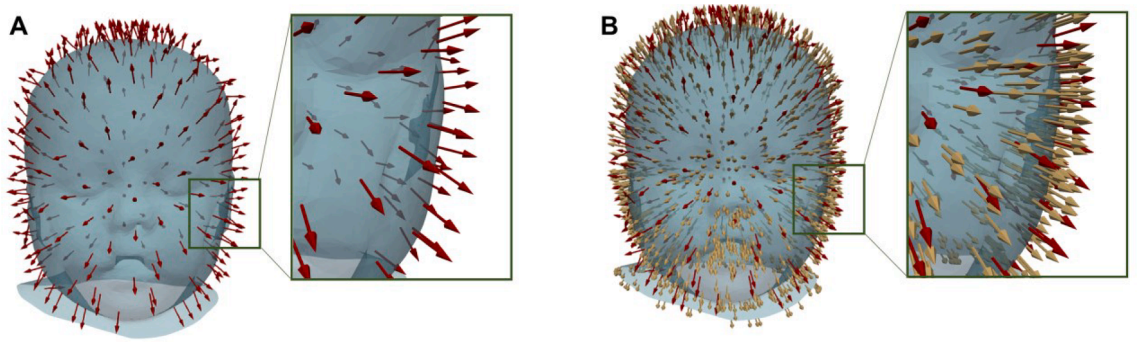

Fig. 5. Displacement fields for head transformation. (A) Sparse displacement field in red arrows; (B) Dense displacement field in gold arrows.

one of the populated N positions such as $\mu_i = (x_i, y_i, z_i)$, a global distribution $g(p_j)$ can be estimated as:

$$g(p_j) = \sum_{i=1}^{N} \lambda_i g_i(p_j; \mu_i, \sigma_i), \tag{3}$$

where $g(p_j)$ is a mixture of the N component distributions and λ_i is the mixing weights with $\lambda_i > 0$ and $\sum_i \lambda_i = 1$. In practice, this process consists in applying a gaussian distribution at each point of the point-based head model M_m, and computing an overall distribution for the entire head surface by performing the weighted sum of the distributions. Using this mixture of components concept, the dense displacement field, $\{u_d, v_d, k_d\}$, is computed by convolving the sparse displacement field with each g_i distribution such as:

$$\{u_d(p_j), v_d(p_j), k_d(p_j)\} = \{u_s(p_j), v_s(p_j), k_s(p_j)\} * g(p_j), \tag{4}$$

with $\lambda_i = 1/n$. Ultimately, this approach allows generating a smooth populated dense displacement field from the partial populated sparse one. This dense displacement field is applied to the original head surface to perform the surface warping.

2.3.2. Transformation regularization

Due to the interpolation properties of the dense displacement field estimation procedure, specific head features, namely the facial ones, can be oversmoothed during the transformation process. To avoid this issue, a weighted regularization term that acts like an anatomical constraint is added to the dense displacement field. The constrained displacement field $\{u_c, v_c, k_c\}$ can be defined for each point p_j as:

$$\{u_c(p_j), v_c(p_j), k_c(p_j)\} = \alpha(j) \times \{u_d(p_j), v_d(p_j), k_d(p_j)\} + (1 - \alpha(j)) \times r(p_j). \tag{5}$$

where α is a weight factor and $r(p_j)$ represents a regularization term that restricts the smoothing of the facial region. Specifically, the regularization is accomplished by ensuring the same motion values for all the facial points, allowing the movement of the main facial region as a whole and, therefore, preserving the facial features. For that, the motion displacement of a particular facial landmark, *i.e.* the Sellion (SL), was used as regularization term, being this term defined as $r(p_j) = \{u(sl), v_d(p_j), k_d(p_j)\}$. $u(sl)$ represents the motion value for the SL landmark in the first direction. Since only this specific motion direction is used for the regularization, a certain degree of flexibility of the augmentation for the regularized region is obtained.

The weight factor α is used to control the influence of each term of equation (5) in the estimation of the constrained displacement field, so that the following conditions are ensured during the transformation process:

1. The regularization term must only affect the facial region;
2. The original dense displacement field should be maintained for the remaining regions of the head;
3. Abrupt changes in motion displacement values for neighboring points should be avoided.

To compute the weight $\alpha(j)$ for each surface point, a two-stage strategy is applied. Firstly, the head surface is roughly divided by a plane into two different regions: 1) the cranial region, including the occipital, parietal, and frontal head regions; and 2) the facial region. The separation plane is computed using labeled anthropometric landmarks of the head. In the second stage, weights are estimated for each point of the surface according to its position on the head in relation to the separation plane. Let us define the initial weight of a point j as:

$$w_j = (p_j - \boldsymbol{o}) \bullet \widehat{\mathbf{N}} \tag{6}$$

where $\widehat{\mathbf{N}}$ is the unit normal vector of the separation plane that passes through the origin of the head $\boldsymbol{o}$. Implicitly, w_j represents the signed distance between the j-th point of the head surface and the separation plane, having positive values for the points above the plane, *i.e.,* points belonging to the cranial region, and negative values for the ones below, *i.e.,* points of the facial region. To compute the final weight α_j, a sigmoid function is applied to the initial weight such as:

$$\alpha_j = f(w_j) = \frac{1}{1 - e^{-\beta w_j}}, \tag{7}$$

where β controls the slope of the sigmoid curve. By applying the sigmoid function, the weight is normalized to be within the range [0–1], having a value near one in points of the cranial region and smoothly decreasing to zero for the points in the facial region. In this sense, the regularization term is strongly applied to the facial region and neglected for the cranial region.

2.3.3. Head transformation process

During the head transformation process, the computation of the displacement fields as described in the previous sections is performed iteratively. At each iteration, new head surface points, $p_j^{'}$, are computed as:

$$p_j^{'} = p_j + \{u_c(p_j), v_c(p_j), k_c(p_j)\}. \tag{8}$$

At each iteration t, the evolution of the head surface towards the target model is performed by minimizing an energy function given as:

$$F = \sum_{i=1}^{N} ||p_{mi}^{'} - p_{ti}|| \tag{9}$$

where $p_{mi}^{'}$ is the updated position of the i-th point of the point-based head model of the moving head and p_{ti} are the target coordinates. This procedure is performed until a minimum value defined for F is reached or during a fixed number of iterations.

Overall, the application of the proposed methodology allows generating different head shapes according to the chosen target p3DMM and to the selected variation mode of the model. Plus, once a controlled target model is defined, unrealistic augmented surfaces are avoided. Moreover, the use of control points as a reference to perform the global transformation allows providing flexibility to the augmentation process since dense point-to-point transformations that would restrict the final surface point positions are avoided.

3. Experiments

To validate the proposed data augmentation method, three evaluation analyses were performed. Firstly, the intrinsic representativeness of the constructed p3DMMs is validated. Secondly, a qualitative analysis where the augmented surfaces were visually inspected is performed. Finally, the performance of different DL approaches using the proposed augmentation is studied.

3.1. Head surfaces dataset

A dataset of 3D head surfaces was used for the validation of the proposed method. The head surfaces were generated from Magnetic Resonance images using the approach described in [34]. Data were obtained as part of routine clinical care during hospital treatment and were retrospectively processed for this work. Ethical approval was given by the ethics committee of the Medical Faculty Carl Gustav Carus of the Technical University Dresden to analyze the routine clinical data. The need for specific parental consent was waived by the ethics committee since only anonymized data are analyzed.

Each head surface contained manually labeled anthropometric landmarks (Fig. 6), namely: glabella (GL), sellion (SL), subnasal (SN), right and left exocanthions (R-EX/L-EX), and tragions (R-TR/L-TR). The dataset was composed of head shapes with both normal (17 surfaces) and deformed heads (8 with Pl, 45 with Br, 37 with Sc, and 21 with PlBr). For all the subsequent experiments, a three-fold *leave-p-out* cross validation strategy was applied, where head surfaces of each cranial deformity were selected from the initial dataset to be used only as testing data. Specifically, three surfaces of each cranial deformity were selected for the first and second testing datasets, whereas two surfaces of each cranial deformity were selected in the third testing dataset. Thus, overall, a dataset composed of 40 original head surfaces (8 for each one of the five types of cranial deformities) was obtained as the testing dataset. The training datasets were used to compute the p3DMM of each deformity class and to train the DL approaches.

The augmentation method was applied offline to each one of the training head surfaces. For the transformation process, the value of F and the number of iterations were empirically set to 0.005 and 100, respectively. Each head surface was augmented for the cranial deformities different from the original head shape (*e.g.*, a normal head shape is augmented to a Pl, a Br, a Sc, and a PlBr shapes or a Pl shape is augmented to produce a normal, a Br, a Sc, and a PlBr shapes). Thus, each head surface originated four augmented ones, each one with a different cranial deformity. To compute the target deformity to be used in the augmentation approach, the shape variation of the respective p3DMM was randomly chosen. Finally, 100 head surfaces of each cranial deformity were randomly selected from the augmented surfaces, achieving an overall augmented training dataset of 500 head surfaces for each cross-validation folder.

3.2. Intrinsic evaluation of the p3DMMs

In the first evaluation analysis, the proposed p3DMM is validated. For that, three evaluation metrics commonly used in the literature were used, namely *compactness*, *generalization*, and *specificity* [33,35]. Compactness measures the percentage of variance of the training data that is explained by the statistical model. In this work, we evaluate the p3MMs by retaining the modes of variation that explains at least 95% of the variance. Concerning the generalization, this metric measures the ability of the statistical model to generate new shapes that were not used to construct the statistical model. To calculate the generalization error for each p3DMM, we project the point-based models of the testing shapes of the respective cranial deformity to the PCA space of the statistical model from which they were excluded and measure the distance between the original point-based model and its projection. Particularly, the per-point Euclidean distance was calculated and the average value over all testing shapes and points was retrieved. Finally, specificity metric evaluates the plausibility of the new shapes that are generated using the statistical model. To calculate this measure, 100 random point-based models were generated from each p3DMM, and their Euclidean

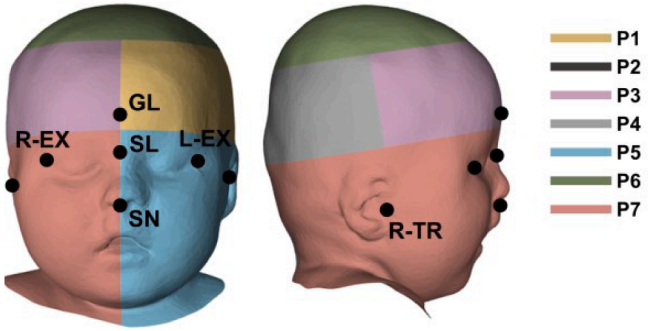

Fig. 6. Anthropometric landmarks and division of the head by segmentation regions.

distance to the closest model of the training set was computed.

3.3. Visual evaluation of deformed surfaces

In the second evaluation analysis, the realism of the heads generated using the proposed augmentation approach is evaluated. Specifically, it was studied if one given augmented surface is not easily perceived or distinguished from its original head. For that, four experienced observers were presented with 100 pairs of head shapes, each composed of an original head surface and its augmented version, and were challenged to select the original one for each pair. The observers consisted of experienced observers with experience in head shape analysis. To perform the evaluation, the percentage of correctly selected original heads was retrieved and the inner-rater agreement between the observers was calculated using the Krippendorff's alpha score.

3.4. Use of data for deep learning approaches

In the final evaluation analysis, the performance of three different DL-approaches trained using the proposed augmentation is evaluated and compared with the baseline experiment, where data augmentation is not applied. Moreover, the proposed augmentation is compared with different state-of-the-art augmentation techniques, namely: 1) traditional augmentation based on global transformations; 2) an augmentation based on local transformations; 3) an adversarial learning strategy; and 4) augmentation based on the traditional 3DMM. The traditional data augmentation strategy consisted of applying commonly used jitter, rotations, and scaling transformations to the head surfaces. Concerning the augmentation based on local deformations, the PointWolf (PW) method proposed in [27] was applied. This method uses locally weighted transformations to generate smooth non-rigid deformations of a point-cloud. Here, the augmentation parameters were experimentally chosen to obtain realistic head surfaces. Since adversarial learning strategies already demonstrate their potential to generate artificial data, the PointAugment (PA) method proposed in [26] was also applied in this work for comparison. More specifically, the PA method was used to train an *augmentor* with the ability to augment head surfaces. Firstly, the network was trained to jointly optimize the *augmentor* and a head shape classifier. Once trained the networks, the trained *augmentor* was used to produce augmented head samples. This procedure mimics traditional literature practice where trained generators of Generative Adversarial Networks (GAN) are used to produce synthetic or augmented data [36]. Lastly, an augmentation based on the traditional 3DMM was implemented. Here, a 3DMM was constructed for each cranial deformity using the traditional approach proposed in [31]. From the statistical models, new head instance shapes were obtained and used to generate augmented data.

Since the inherent characteristics of the comparative state-of-the-art augmenters do not define the final type of cranial deformity of an augmented head surface, it can happen that an augmented surface does not have the same deformity as the original one (e.g. due to global or local deformations that may modify the overall head shape). To solve this issue, it was needed to validate the final augmented surfaces to attribute each of them to the correct cranial deformity. For that, a standard clinical guideline was followed, where cranial indexes were extracted automatically from the manually labelled anthropometric landmarks and a classification was attributed according to the indexes [6]. The application of this method allows to avoid incorrect classifications that could affect the training of the DL methods. Finally, for each method, 100 head surfaces of each cranial deformity were generated from the training datasets, achieving a training dataset with 500 head surfaces for each cross-validation folder, similarly to the evaluation experiment of the proposed data augmentation.

3.4.1. Head shape classification

Classification is a common task in computer vision that consists of assigning a label to a given object. In this work, a classification approach is applied to categorize head surfaces according to their cranial deformity. To perform the classification, the neural network PointNet proposed in [25] was used. Thus, the input of the network corresponds to a point cloud of the head surface and the output is the scores for the candidate deformities. By selecting the deformity with the higher score, the head shape class is found. The network configuration used was as described in [25]. The training parameters were fixed for all experiments performed. Specifically, the networks were trained during 200 epochs with a mini-batch size of 10 and using the Adam optimizer with an initial learning rate of 0.001. During the training, the learning rate was updated using a step learning rate decay policy. Finally, the performance of the classification task for the different experiments conducted was assessed in terms of accuracy, precision, recall, and F1-score.

3.4.2. Head shape semantic segmentation

One approach that can be used to evaluate head shape corresponds to analyzing different parts of the head. In computer vision, this can be accomplished by semantically segmenting the head shape. In this work, the semantic segmentation of head shapes was also evaluated using the PointNet framework. For that, the anthropometric landmarks of the head shapes were used to divide the surfaces into seven different regions including the four cranial quadrants proposed in [37], the top region, and the remaining left and right regions. Fig. 6 illustrates the division of the head surface in different regions (P1-P7). The configuration of the network used in this work for semantic segmentation is also described in [25]. Concerning the training procedure for the task of head semantic segmentation, the same training parameters as the ones used for the classification task were used for all the experiments performed. To evaluate the results for segmentation task, the intersection over union (IoU) metric was used.

3.4.3. Anthropometric landmark detection

The most common clinical approach to evaluate head shape relies on the extraction of cranial measurements from anthropometric landmarks of the head [34]. Thus, in this work, the effectiveness of the proposed data augmentation approach to increase the performance of a landmark detector is evaluated. The landmark detector used in the present work was described in [34]. In short, the detection method detects anthropometric landmarks by creating 2D images representative of the 3D head surfaces and by using a DL-approach to detect the landmarks in the 2D representations. Similarly to the classification and semantic segmentation tasks, the landmark detection method was applied for all the evaluations conducted in this work, namely without data augmentation, with the proposed augmentation, and with the comparative state-of-the-art augmentation methods. For all experiments, the same training variables were fixed, using the optimal settings found in the work proposed in [34]. Specifically, the learning rate was set to 0.0004 and 10 images were used for the batch size. For the optimization, the Adam solver was used with a regularization term of 0.01. Finally, the trainings were performed for a fixed number of 250 epochs. To evaluate the landmark detection task, the mean error was computed, which corresponds to the Euclidean distance between the detected landmark and the ground-truth.

4. Results

4.1. Intrinsic evaluation of the p3DMMs

The average compactness for the three cross-validation folders is presented in Table 1. In the first row of Fig. 7, the generalization error of each p3DMM for a given number of principal components retained is presented. In the second raw of the figure, the specificity is given. Note that since all point-based models were initially normalized to be contained in a unit sphere, the Euclidean distances presented in Fig. 7 are normalized.

Table 1
Number of principal components to explain 95% of the training set (average of the three-fold).

P3DMM	Training shapes	Components
N	14	8
Pl	5	4
Br	42	12
Sc	34	12
PlBr	18	10

4.2. Visual evaluation of deformed surfaces

In the visual inspection, the percentage of correctly selected original heads obtained was only 56% (45%, 64%, 68%, and 47% for the different observers). Moreover, the inner-rater agreement score obtained was 0.02. Fig. 8 shows examples of augmented surfaces generated from different original head shapes (Please see Appendix A for further information).

4.3. Use of data for deep learning approaches

In this subsection, the experiments' results of the different deep learning approaches are presented. Table 2 reports the performance of the PointNet for head shape classification when trained without data augmentation, with the proposed augmentation, and with the other comparative augmentation approaches. In the table, it is presented the performance evaluation for each cranial deformity class, corresponding to the evaluation of 8 testing shapes for each (totaling the 40 testing head shapes). The corresponding confusion matrix is presented in Fig. 9. Table 3 presents the results related to the performance of the PointNet for semantic segmentation using the proposed augmentation and the remaining comparative approaches. Finally, the performance of the landmark detector is presented in Fig. 10. To evaluate statistically significant differences, a two-tailed paired *t*-test ($p < 0.05$) was applied between each comparative experiment and the proposed augmentation, and the results are presented in the figure.

5. Discussion

In this work, an augmentation method that transforms head surfaces towards different cranial deformities is presented. To the best of the knowledge, this is the first work to address the problem of the creation of head surfaces describing different cranial deformities. The validation of the proposed method was divided into two parts: (1), the representativeness of the proposed p3DMM was explored, and (2), the augmented strategy and their advantages to train DL-based approaches were evaluated. Concerning the intrinsic evaluation of the p3DMM, an ideal statistical model should be compact, general, and specific. Analysing Table 1, one can conclude that the p3DMMs can be considered sufficiently compact since few components are able to describe the variability of the dataset. A good generalization capability was also found for the p3DMMs (Fig. 7), since lower errors in the generalization ability

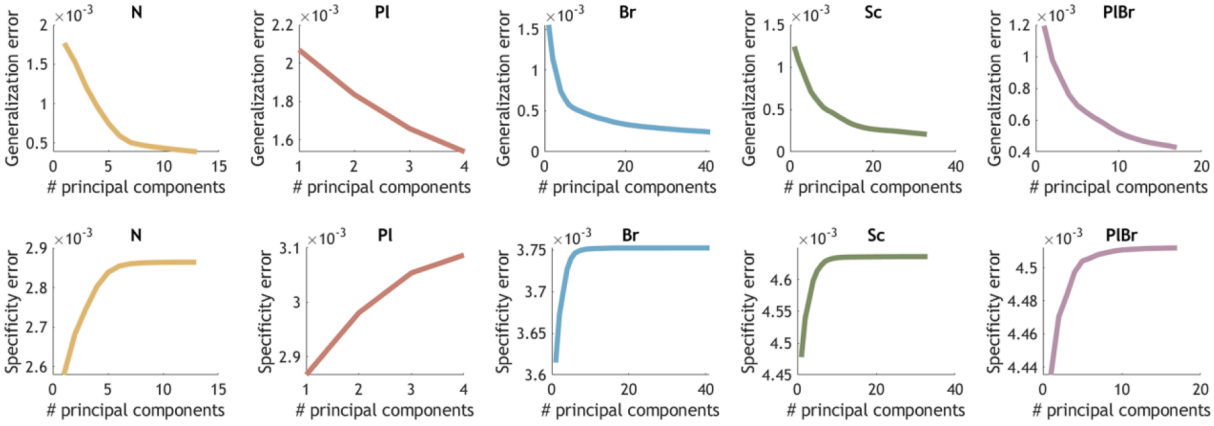

Fig. 7. Characteristics of the cranial deformity p3DMMs. First row: normalized generalization; Second row: normalized specificity.

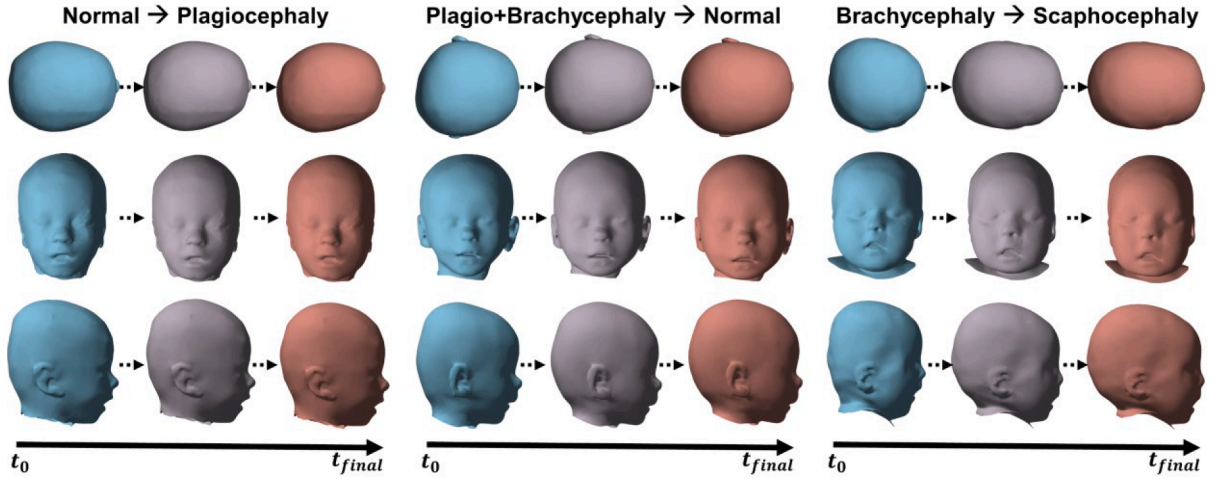

Fig. 8. Examples of transformed heads. Blue surfaces represent the original head and red surfaces represent the final transformed head. The purple surfaces represent the head during an intermediate iteration of the transformation process. First row: top view; Second row: frontal view; Third row: lateral view.

Table 2
Head shape classification performance (%). Bold values indicate the best performance.

	Accuracy					
	N	**Pl**	**Br**	**Sc**	**PlBr**	**Mean**
Baseline	50.0	12.5	62.5	75.0	**87.5**	57.5
Traditional	62.5	37.5	75.0	87.5	62.5	65.0
PW	**75.0**	50.0	75.0	75.0	50.0	65.0
PA	62.5	25.0	62.5	75.0	75.0	60.0
3DMM	50.0	12.5	87.5	**100.0**	75.0	65.0
Proposed	50.0	**62.5**	**100.0**	87.5	**87.5**	**77.5**
	Precision					
	N	**Pl**	**Br**	**Sc**	**PlBr**	**Mean**
Baseline	36.4	**100.0**	**100.0**	60.0	53.8	70.0
Traditional	50.0	60.0	60.0	**100.0**	62.5	66.5
PW	50.0	57.1	66.7	85.7	80.0	67.9
PA	50.0	66.7	50.0	85.7	60.0	62.5
3DMM	50.0	33.3	55.6	77.8	45.5	52.4
Proposed	**80.0**	83.3	61.5	87.5	**87.5**	**80.0**
	Recall					
	N	**Pl**	**Br**	**Sc**	**PlBr**	**Mean**
Baseline	50.0	12.5	62.5	75.0	**87.5**	57.5
Traditional	62.5	37.5	75.0	**87.5**	62.5	65.0
PW	**75.0**	50.0	75.0	75.0	50.0	65.0
PA	62.5	25.0	62.5	75.0	75.0	60.0
3DMM	50.0	12.5	62.5	**87.5**	62.5	55.0
Proposed	50.0	**62.5**	**100.0**	**87.5**	**87.5**	**77.5**
	F1-Score					
	N	**Pl**	**Br**	**Sc**	**PlBr**	**Mean**
Baseline	42.1	22.2	**76.9**	66.7	66.7	54.9
Traditional	55.6	46.2	66.7	93.3	62.5	64.8
PW	60.0	53.3	70.6	80.0	61.5	65.1
PA	55.6	36.4	55.6	80.0	66.7	58.8
3DMM	50.0	18.2	58.8	82.4	52.6	52.4
Proposed	**61.5**	**71.4**	76.2	**87.5**	**87.5**	**76.8**

were found. This means that the used models are capable of representing new shapes. Moreover, the fact that the generalization error only decreases moderately after few components for the majority of the p3DMMs, suggests that the benefit of choosing more components is not too much representative. This corroborates that the models are compact. However, higher generalization errors were found for the p3DMM corresponding to the Pl deformity. This is somehow expected since a small number of point-based models were used to construct the statistical model. However, even this p3DMM showed to produce accurate new instances of the model, since its specificity demonstrate the quality of the randomly generated point-based models and their similarity to the training models. Thus, overall, the results obtained showed the efficiency of the proposed p3DMM. Nevertheless, despite the validity of the statistical model had been verified, new head surfaces can be included in the p3DMM construction to increase their representativeness, and therefore, potentiate the generation of different head shapes. It is also important to emphasize that since the instances of the point-based models are only used to create controls points to augment a given head shape towards a deformity, the same target point-based model can generate multiple augmented surfaces if different moving heads and different transformation parameters, *i.e.* number of iterations, were used.

For the evaluation of the augmented surfaces, we started by inspecting them visually and establishing a comparison with their original forms to test if they are easily distinguishable. Overall, it was proven that the augmented surfaces are realistic and comparable to the original surfaces, since the percentage of correctly selected original shapes was only 56%. Moreover, the inter-rater score near to zero showed that there is no agreement between the observers beyond chance. Together, both metrics suggest a randomness in the process of original head shape selection, since no selection criteria that allowed to completely distinguish the original surfaces from the augmented ones was observed. This suggests that the augmented surfaces are similar to real head shapes and therefore are indistinguishable from them. In fact, the example surfaces presented in Fig. 8 show that very realistic heads are generated. Our strategy based on a transformation process towards an anatomically correct target shape proved to be robust to prevent abnormal head shapes. Our facial regularization strategy also proved to be crucial to prevent oversmoothed surfaces at the face region (Fig. 11). Moreover, Fig. 8 also demonstrated that our method is effective to correctly generate the different head deformities, *i.e.,* the method can transform cranial deformed heads to normal ones, normal heads to deformed ones, and can also change the deformity type of a pathological head. This results from the fact that specific target deformities are used in this work. Indeed, the definition of the final deformity of an

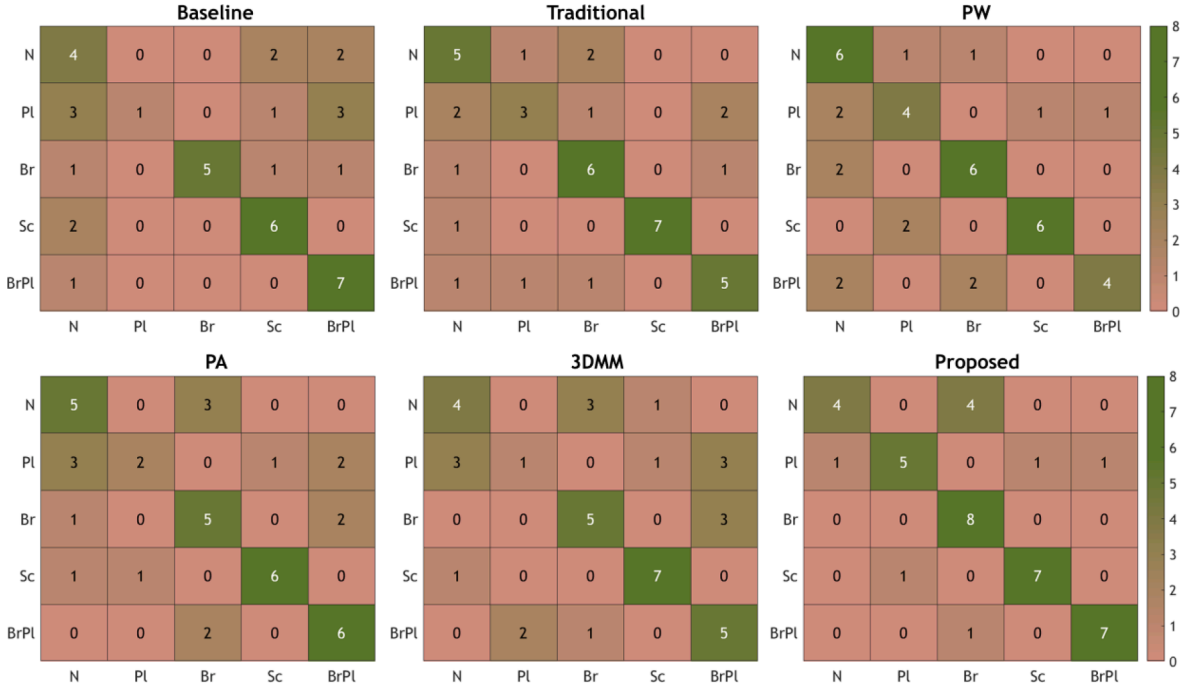

Fig. 9. Confusion matrix of the head shape classification for the different experiments performed.

Table 3
Head shape semantic segmentation results in terms of IoU (%). Bold values indicate the best performance.

Dataset	P1	P2	P3	P4	P5	P6	P7	Mean
Baseline	87.3	82.6	87.8	82.5	94.6	91.2	94.6	88.7
Traditional	85.3	80.5	85.1	81.9	93.1	90.8	93.2	87.1
PW	**88.6**	**84.3**	**88.3**	**84.5**	**95.0**	**91.9**	**95.1**	**89.7**
PA	86.0	78.0	85.1	79.2	93.2	89.0	93.0	86.2
3DMM	85.9	81.8	85.7	81.7	94.2	90.2	94.2	87.7
Proposed	88.0	83.9	87.3	83.7	94.8	91.7	94.7	89.2

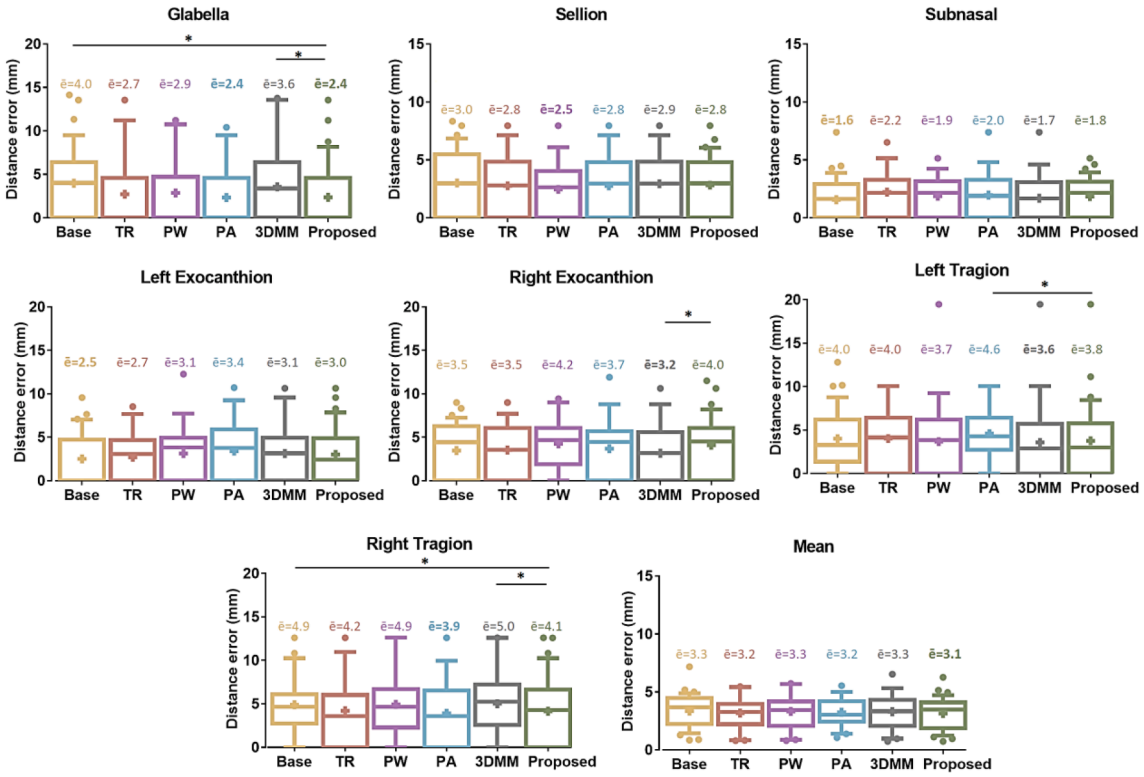

Fig. 10. Landmark detection performance. The ends of the whiskers represent the 10th and 90th percentiles. The crosses represent the average value for each boxplot, with the numeral value indicated above it (ē). The best average values per landmark are in bold. The dot points are outliers. *$p < 0.05$ in a two-tailed paired *t*-test between the proposed augmentation and the remaining experiments.

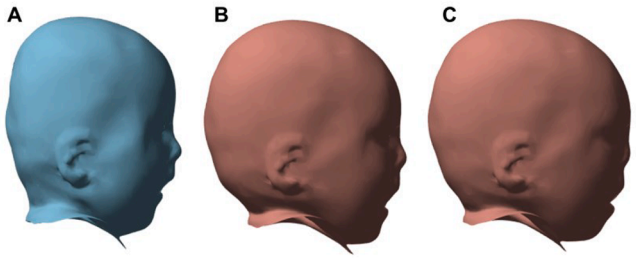

Fig. 11. Influence of regularization term. (A) Original head; (B) Transformed head with regularization term; (C) Transformed head without regularization term.

augmented shape is performed by selecting the intended p3DMM. Moreover, since the statistical model captures the shape variations of their base models, different target head shapes can be obtained within the same type of deformity (Fig. 4). Additionally, different severities of a specific deformation can be targeted by selecting a p3DMM mode with the desired deformity. Another important aspect of the proposed method is the use of control points to guide the transformation process. If a complete target head surface was used, the final transformed head shape should be strongly restricted to the target one. This means that different original head surfaces would have very similar augmented versions if the same target models were used. Our formulation is purely based on a set of anatomically defined control points that represent the overall shape of a head. However, this formulation does not restrict the final augmentation to a specific surface. This provides flexibility to the augmentation process, once it is only intended to modify the head shape of a given surface, preserving its anatomical features. Thus, augmented surfaces representative of their original versions are generated even if the same target model is used. Moreover, our augmented surfaces proved that the sparse motion field generation strategy and the statistical model effectively allow recovering the target deformity once the expected final deformities were achieved. Furthermore, the strategy used to estimate the dense motion field showed to accurately recover the transformation for the entire head, since smooth transformations between neighbouring points were obtained [38]. As a remark, a visual inspection study was also conducted for the comparative literature augmentation approaches, being the results presented in the Appendix B.

Besides the visual evaluation of the augmented surfaces, the effectiveness of the augmentation approach to improve the accuracy of

different DL methodologies was also evaluated. The first evaluated method was the classification of the heads concerning their cranial deformity using the well-known PointNet configuration [25]. To the best of the knowledge, it is the first time that a direct classification of a 3D head shape concerning cranial deformities is assessed. Our results with augmented data clearly outperformed the non-augmented strategy, with a mean accuracy improvement of 20%. The proposed data augmentation approach increased the size and variability of the training dataset, allowing to improve the generalization of the model and achieving better classification. This can be easily perceived by evaluating the classification accuracy for the Pl category. During training without data augmentation, only few surfaces of this category were used, achieving inaccurate classifications on the testing dataset (12.5%). When using data augmentation, head shapes with different deformities can be transformed to achieve Pl deformities, allowing to increase the number of head surfaces with this deformity seen during the training process and improving the final classification. One should note that a few number of head surfaces with Pl was used to construct the statistical model representative of this population, and thus, few modes of variation can be retrieved from it. This means that the number of target shapes is also limited. Nevertheless, the classification results suggest that variable head surfaces with this deformity were achieved using the proposed augmentation method, proving the effectiveness of the proposed augmentation even when having a small number of shapes with a given deformity. Thus, even if a low number of data are initially available, the proposed augmentation has the potential to increase the size and variability of the dataset. Besides the improvement in comparison with training without data augmentation, the proposed augmentation also showed to outperform the other state-of-the-art augmentation methods. A higher mean accuracy for the classification was achieved by training with the proposed augmentation. Comparing with the traditional augmentation, with the PW, and with the PA methodologies, our method has as a clear advantage the targeting of specific deformations, instead of randomly transform the surface. This characteristic of the method allows to control the final head shape, allowing to obtain augmented surfaces more realistic than the ones obtained with the remaining methods (please see Appendix B for further details). Moreover, for the use-case of classifying a head concerning the cranial deformity, this characteristic of the proposed method is paramount to achieve a good performance of the method. Moreover, even if only normal shapes are initially available from training the classification method, the proposed approach can generate different deformities from them, if we assume that the deformity-specific p3DMMs are priorly constructed, which is not possible with state-of-the-art augmentation. Comparing with the traditional 3DMM, this approach also allows to produce head shapes with specific deformities, but the produced head shapes are limited by the anatomical variability captured by the statistical model, whereas our proposed approach can generate a high number of head surfaces for the same variation mode of the statistical model, as abovementioned.

Another important analysis that can be retrieved from the classification results is that a performance improvement was not verified for the normal class when using our approach. Despite having better precision when compared with the remaining experiments, the recall obtained for the normal class was low, meaning that there are normal heads that are being wrongly classified with a different head shape. Analysing the confusion matrix of Fig. 9, it is possible to verify that the normal head shapes are being classified as brachycephaly. This can be explained by the fact that the normal heads and the brachycephaly ones differ in the ratio between the cranial width and length, being their ground-truth classification based on a threshold value applied to the ratio. This implies that exists a transitional region between the normal head shape and the brachycephaly condition. In the training datasets, it was verified that the number of normal training head shapes near to the transition region is low, whereas the number of brachycephaly shapes in their side of the transition region is high. This can promote that normal testing head shapes with a ratio near to the transition region being classified as brachycephaly. To solve this issue, and to improve the overall performance of the method for all diagnostic classes, more surfaces near to transitional diagnostic regions must be used to create the respective p3DMM, therefore enabling the creation of augmented surfaces at these regions.

As a second experiment, the task of semantic segmentation of head surfaces also showed to benefit from the use of the proposed data augmentation. Table 3 demonstrated the improvement of the state-of-the-art segmentation approach when augmented surfaces are used. Specifically, higher IoU was achieved for the head parts in comparison with the baseline study, *i.e.* without data augmentation. Moreover, when compared with the remaining augmentation approaches, it was verified that the proposed approach was better than the majority of the comparative methods, including traditional augmentation, the PA, and the 3DMM-based augmentation. However, the PW augmentation produced slightly better results for the task of head shape classification. This can be explained by the fact that they are applying local deformations to the different head regions, which can increase their variability and, therefore, can potentiate the semantic segmentation. Nevertheless, the obtained results demonstrated that the proposed augmentation approach also generates quality data to be used for semantic segmentation. Here, the performance improvement using the proposed augmentation is higher for the classification task, which can be explained once the proposed augmentation has the goal of generating different cranial deformities, having a higher impact on the categorization of the head concerning its overall shape. For landmark detection, Fig. 10 shows the improvement for this task using the proposed augmented surfaces, in comparison with all studies performed. Indeed, when using the proposed augmentation, the performance of the detection was better than all the comparative methods for the majority of the landmarks. Moreover, the lowest mean distance error (3.1 mm) was obtained when using our augmented surfaces for training, indicating superior performance of the detection with the augmentation approach.

As a final remark, despite the most common types of cranial deformities were addressed in this work, the proposed method can be easily expanded to obtain head surfaces with other cranial deformities, being only needed to add examples of head shapes with the deformity to create the proposed p3DMM.

6. Conclusion

In this work, a novel methodology to augment 3D head surfaces to be used during training processes was presented. Specifically, instead of performing random transformations that are not enough to increase the variability of the training dataset, the augmentation of head surfaces towards different deformities was targeted. Our results proved that the augmented surfaces are indistinguishable of the real clinical ones. Moreover, quantitative analysis proved that our augmented strategy increased the accuracy of state-of-the-art DL algorithms. Overall, the effectiveness of the augmentation method to generate head surfaces with different deformities was proved, suggesting the added value of the method to be used in the development of the automatic methods for head shape evaluation.

CRediT authorship contribution statement

Helena R. Torres: Conceptualization, Methodology, Software, Validation, Investigation, Writing – original draft, Writing – review & editing. **Bruno Oliveira:** Methodology, Writing – review & editing. **Pedro Morais:** Methodology, Writing – review & editing. **Anne Fritze:** Resources, Writing – review & editing. **Mario Rüdiger:** Resources, Writing – review & editing. **Jaime C. Fonseca:** Supervision, Funding acquisition, Writing – review & editing. **João L. Vilaça:** Supervision, Funding acquisition, Writing – review & editing.

Declaration of Competing Interest

The authors declare that they have no known competing financial interests or personal relationships that could have appeared to influence the work reported in this paper.

Acknowledgements

This work was funded by projects "NORTE-01-0145-FEDER-000059" and "NORTE-01-0145-FEDER-000045", supported by Northern Portugal Regional Operational Programme (Norte2020), under the Portugal 2020 Partnership Agreement, through the European Regional Development Fund (FEDER). It was also funded by national funds, through the FCT – Fundação para a Ciência e Tecnologia within the R&D Units Project Scope: UIDB/00319/2020 and by FCT and FCT/MCTES in the scope of the projects UIDB/05549/2020 and UIDP/05549/2020. The authors also acknowledge support from FCT and the European Social Found, through Programa Operacional Capital Humano (POCH), in the scope of the PhD grant SFRH/BD/136670/2018 and SFRH/BD/136721/2018.

Appendix A. Multimedia material

An animation showing the transformation of a given head model towards different deformities can be seen in the multimedia material of this manuscript.

Appendix B. Qualitative analysis of state-of-the-art augmentation methods

Examples of head surfaces augmented with the comparative state-of-the-art augmentation methods evaluated in this work can be found as supplementary material.

Appendix C. Supplementary material

Supplementary data to this article can be found online at https://doi.org/10.1016/j.jbi.2022.104121.

References

[1] J.L.Y. Cheong, et al., Brain volumes at term-equivalent age are associated with 2-year neurodevelopment in moderate and late preterm children, J. Pediatr. 174 (2016) 91–97.e1.
[2] A.L.C. Martiniuk, C. Vujovich-Dunn, M. Park, W. Yu, B.R. Lucas, Plagiocephaly and developmental delay: a systematic review, J. Dev. Behav. Pediatr. 38 (1) (2017) 67–78.
[3] R.I. Miller, S.K. Clarren, Long-term developmental outcomes in patients with deformational plagiocephaly, Pediatrics 105 (2) (2000) e26.
[4] G.F. Rogers, Deformational plagiocephaly, brachycephaly, and scaphocephaly. Part I: Terminology, diagnosis, and etiopathogenesis, J. Craniofac. Surg. 22 (1) (2011) 9–16.
[5] Kanlaya Ditthakasem, J. C. K. D, Deformational Plagiocephaly: A Review, Pedriatric Nurs. 43(2) (2017) 59–65.
[6] J.F. Wilbrand, et al., Clinical classification of infant nonsynostotic cranial deformity, J. Pediatr. 161 (6) (2012) 1120–1125.e1.
[7] F. Di Rocco, V. Ble, P.A. Beuriat, A. Szathmari, L.N. Lohkamp, C. Mottolese, Prevalence and severity of positional plagiocephaly in children and adolescents, Acta Neurochir. (Wien) 161 (6) (2019) 1095–1098.
[8] S. Ifflaender, M. Rüdiger, D. Konstantelos, K. Wahls, W. Burkhardt, Early Human Development Prevalence of head deformities in preterm infants at term equivalent age ☆, Early Hum. Dev. 89 (2013) 1041–1047.
[9] H.R. Torres, et al., Developing a medical training game for visual assessment of head deformities in infants. SeGAH 2021–2021 IEEE 9th International Conference on Serious Games and Applications for Health, 2021.
[10] F. Veloso, et al., Synthetic infant head shapes with deformational plagiocephaly: concept and 3D model parameterization. International Conference on Serious Games and Applications for Health, 2019.
[11] H. Aarnivala, et al., Accuracy of measurements used to quantify cranial asymmetry in deformational plagiocephaly, J. Cranio-Maxillofacial Surg. 45 (8) (2017) 1349–1356.
[12] H.R. Torres, et al., Anthropometric landmarking for diagnosis of cranial deformities: validation of an automatic approach and comparison with intra- and interobserver variability, Ann. Biomed. Eng. (2022).
[13] M. Bakator, D. Radosav, Deep learning and medical diagnosis: a review of literature, Multimodal Technol. Interact. 2(3) (2018).
[14] J. Ker, L. Wang, J. Rao, T. Lim, Deep learning applications in medical image analysis, IEEE Access 6 (2017) 9375–9379.
[15] H.R. Torres et al., Deep learning-based detection of anthropometric landmarks in 3D infants head models, in: SPIE Medical Imaging, 2019, no. March, p. 112.
[16] J. Booth, A. Roussos, A. Ponniah, D. Dunaway, S. Zafeiriou, Large Scale 3D Morphable Models, Int. J. Comput. Vis. 126 (2–4) (2018) 233–254.
[17] P. Jonathon Phillips, P.J. Flynn, T. Scruggs, K.W. Bowyer, W. Worek, "Preliminary face recognition grand challenge results, FGR 2006 Proc 7th Int. Conf. Autom. Face Gesture Recognit. (2006) 15–21.
[18] A. Savran et al., Bosphorus database for 3D face analysis, Lect. Notes Comput. Sci. (including Subser. Lect. Notes Artif. Intell. Lect. Notes Bioinformatics), vol. 5372 LNCS, pp. 47–56, 2008.
[19] P. Paysan, R. Knothe, B. Amberg, S. Romdhani, T. Vetter, A 3D face model for pose and illumination invariant face recognition, 6th IEEE Int Conf. Adv. Video Signal Based Surveillance, AVSS (2009, 2009,) 296–301.
[20] H. Dai, N. Pears, W. Smith, C. Duncan, Statistical modeling of craniofacial shape and texture, Int. J. Comput. Vis. 128 (2) (2020) 547–571.
[21] T. Li, T. Bolkart, M.J. Black, H. Li, J. Romero, Learning a model of facial shape and expression from 4D scans, ACM Trans. Graph. 36 (6) (2017) 1–17.
[22] S. Ploumpis, H. Wang, N. Pears, W. A. P. Smith, S. Zafeiriou, Combining 3D morphable models: a large scale face-and-head model.
[23] R. M.I., N. S., Z.A., Deep Learning for Medical Image Processing: Overview, Challenges and the Future. Springer, Cham, 2018.
[24] C. Shorten, T.M. Khoshgoftaar, A survey on Image Data Augmentation for Deep Learning, J. Big Data, vol. 6, no. 1, 2019.
[25] C. R. Qi, H. Su, K. Mo, and L. J. Guibas, PointNet: Deep learning on point sets for 3D classification and segmentation, in: Proc. - 30th IEEE Conf. Comput. Vis. Pattern Recognition, CVPR 2017, vol. 2017-Janua, pp. 77–85, 2017.
[26] R. Li, X. Li, P.A. Heng, C.W. Fu, PointAugment: an auto-augmentation framework for point cloud classification, Proc. IEEE Comput. Soc. Conf. Comput. Vis. Pattern Recognit. (2020) 6377–6386.
[27] S. Kim, S. Lee, D. Hwang, J. Lee, S.J. Hwang, H.J. Kim, Point cloud augmentation with weighted local transformations, in: Proceedings of the IEEE/CVF International Conference on Computer Vision, 2021, pp. 548–557.
[28] Y. Chen, et al., PointMixup: augmentation for point clouds, Lect. Notes Comput. Sci. (including Subser. Lect. Notes Artif. Intell. Lect. Notes Bioinformatics) 12348 LNCS (2020) 330–345.
[29] J. Kittler, P. Huber, Z.-H. Feng, G. Hu, W. Christmas, 3D morphable face models and their applications, International Conference on Articulated Motion and Deformable Objects 1 (2016) 185–206.
[30] B. Egger et al., 3D Morphable face models - Past, present and future, arXiv, 2019.
[31] V. Blanz, T. Vetter, A morphable model for the synthesis of 3D faces, Proc. 26th Annu. Conf. Comput. Graph. Interact. Tech. SIGGRAPH (1999) 187–194.
[32] T. Möller, B. Trumbore, Fast, minimum storage ray-triangle intersection, J. Graph. Tools 2 (1) (1997) 21–28.
[33] R. Davies, C. Twining, C. Taylor, Statistical Models of Shape: Optimisation and Evaluation, Springer Science & Business Media, 2008.
[34] H.R. Torres et al. Anthropometric landmark detection in 3D head surfaces using a rotation-invariant deep learning-based approach, IEEE J. Biomed. Heal. Informatics 2194 (2020).
[35] A. Brunton, A. Salazar, T. Bolkart, S. Wuhrer, Review of statistical shape spaces for 3D data with comparative analysis for human faces, Comput. Vis. Image Underst. 128 (2014) 1–17.
[36] X. Yi, E. Walia, P. Babyn, Generative adversarial network in medical imaging: a review, Med. Image Anal. 58 (2019).
[37] L.H. Plank, B. Giavedoni, J.R. Lombardo, M.D. Geil, A. Reisner, Comparison of infant head shape changes in deformational plagiocephaly following treatment with a cranial remolding orthosis using a noninvasive laser shape digitizer, J. Craniofac. Surg. 17 (6) (2006) 1084–1091.
[38] P. Morais, et al., Dense motion field estimation from myocardialboundary displacements, Int. J. Numer. Method. Biomed. Eng. 32 (9) (2016), e02758.